Current Optics and Photonics
Vol. 1, No. 3, June 2017, pp. 221-227

ISSN: 2508-7266(Print) / ISSN: 2508-7274(Online)
DOI: https://doi.org/10.3807/COPP.2017.1.3.221

Numerical Analysis of Working Distance of Square-shaped Beam Homogenizer for Laser Shock Peening

Taeshin Kim, Seungjin Hwang, Kyung Hee Hong, and Tae Jun Yu*

Department of Advanced Green Energy and Engineering, Handong Global University, Pohang 37554, Korea

(Received March 23, 2017 : revised April 19, 2017 : accepted April 23, 2017)

To apply a square-shaped beam homogenizer to laser shock peening, it should be designed with a long working distance and by considering metal targets with various shapes and textures. For long working distances, a square-shaped beam homogenizer with a long depth of focus is required. In the range of working distance, the laser beam is required to have not only high efficiency but high uniformity, in other words, a good peening quality is guaranteed. In this study, we defined this range as the working distance for laser shock peening. We have simulated the effect of some parameters on the working distance. The parameters include the focal length of the condenser lens, pitch size of the array lens, and plasma threshold of the metal. The simulation was performed through numerical analysis by considering the diffraction effect.

Keywords : Beam homogenizer, Depth of focus, Depth of uniformity, Working distance, Laser shock peening
OCIS codes : (140.3300) Laser beam shaping; (140.3390) Laser materials processing; (160.3900) Metals;

I. INTRODUCTION

Laser shock peening (LSP) enhances metal properties through high power laser pulses resulting in compressive residual stress on the metal surface. The intense laser pulse creates plasma on the metal surface and propagates shock waves through the metal target. The traveling shock wave compresses the lattice structure of the metal. The properties of the metal, such as high cycle fatigue, wear resistance, corrosion resistance and resistance to foreign object debris, are improved [1]. Recently, the application of uniform and square laser beams for LSP has been studied [2]. A uniform beam is helpful for the generation of uniform plasma and compressive residual stress [1, 3]. The square beam also provides minimized overlapping ratio of the adjacent laser beam spot and good surface-covering efficiency on a complex-shaped target [1-5]. Therefore, the square-shaped beam homogenizer, which simultaneously transforms arbitrary and nonuniform beams into uniform square beams, can be used in the LSP.

The metal targets requiring peening may have various forms, heights, and textures. In consideration of the target diversity, a long working distance (WD) is critical for a square-shaped beam homogenizer in the LSP industrial site. The long WD allows various metal targets, indicating that the image distance tolerance of the square-shaped beam homogenizer is insensitive to the defocused position [6]. The WD is deeply related to the depth of focus (DOF) of the square-shaped beam homogenizer. Therefore, the square-shaped beam homogenizer should be designed to comprise a long DOF. Unlike conventional DOF, in which tolerance for the defocused image of a general optical imaging system, plasma threshold should be considered in the LSP. In our previous study, we defined the DOF in the case of the LSP (LSP-DOF) in which the possible range of LSP energy efficiency is over 0.5 [7]. However, although the spatial beam distribution near the target is improper for the LSP, the energy efficiency is calculated as over 0.5 in certain conditions of a square-shaped beam homogenizer system. As the application of the LSP-DOF to this condition is inappropriate, it is necessary to limit the LSP-DOF.

In this paper, we analyzed the range of square beam uniformity over the plasma threshold. The square-shaped

*Corresponding author: taejunyu@handong.edu
Color versions of one or more of the figures in this paper are available online.

beam homogenizer was formed numerically and the diffraction effect was considered in the simulation, unlike in the previous LSP-DOF research [7]. The uniformity of the square beam was obtained at each defocus position near the target. Furthermore, we defined the depth of uniformity (DOU) in the case of the LSP (LSP-DOU) as a high uniformity maintained range with values less than a certain root mean square (RMS) value. We defined the WD for the LSP (LSP-WD) as the overlapping range of the LSP-DOF and LSP-DOU. As the LSP-WD fulfills both the LSP-DOF and LSP-DOU, we can consider LSP-WD as the energy efficient and quality-guaranteed range of the square beam for LSP.

The remainder of this paper is organized as follows. Section 2 explains the principle of a square-shaped beam homogenizer in imaging condition. Section 3 describes the simulation method. The tendency of LSP-DOF, LSP-DOU, and LSP-WD based on some parameters will be discussed in Section 4. The simulation parameters can be divided into the parameters of the square-shaped beam homogenizer and external parameters. For the square-shaped beam homogenizer parameters, we selected focal length (f_c) of the condenser lens and the pitch size (p) of the array lens. For the outer parameter, we chose the plasma threshold intensity (I_{th}).

II. SQUARE-SHAPED BEAM HOMOGENIZER IN IMAGING CONDITION

To transform the arbitrary shape and nonuniform beam into the square and uniform beam simultaneously, we selected a beam homogenizer consisting of two array lenses and one condenser lens. This is advantageous in the application to the LSP with low energy loss compared to a beam homogenizer using diffractive optical elements [8, 9]. Fig. 1 shows the concept of the beam homogenizer.

For the collimated incident beam, the first array lens divides the nonuniform beam into several beamlets, and the second array lens delivers these beamlets to the condenser lens. The condenser lens superposes each beamlet onto an image plane, and a uniform square beam is generated on the image plane [10-12]. The square beam size on the image plane is written as

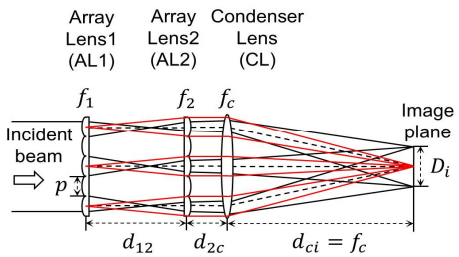

FIG. 1. Concept of the beam homogenizer in imaging condition: (black solid) marginal rays, (black dashed) center lines of each beamlet, and (red solid) chief rays of each beamlet.

$$D_i = p\frac{f_c}{f_1 f_2}\left[(f_1+f_2)-d_{12}\right] \tag{1}$$

$$MP = D_i/p = f_c/f_{eq},\ f_{eq} = \frac{f_1 f_2}{f_1+f_2-d_{12}}, \tag{2}$$

where p is the pitch size of the array lenses, d_{12} is the distance between two array lenses, and f_1, f_2, and f_c are the focal lengths of each lens. The image size is derived from the magnification power (MP), and f_{eq} is the equivalent focal length of the two array lenses. The object distance of this beam homogenizer is zero, and the first array lens plays the role of an object. As the beam homogenizer is a multi-aperture integrator system, a marginal ray passes through the edge of the sub-apertures of the first array lens and the chief ray initiates from the center of the first array lens. When $d_{12} = f_2$, the beam homogenizer fulfills the imaging condition. The red lines in Fig. 1 represent the chief rays in the imaging condition. The ends of the chief rays at the center of each lenslet perfectly correspond with the center of the square image. When the imaging condition $d_{12} = f_2$ is satisfied in Eq. (1), the square beam size (D_i) at the image plane can be simplified as

$$D_i = p f_c/f_2. \tag{3}$$

The beam homogenizer in the imaging condition performs uniform illumination and clear imaging functions simultaneously. The edge steepness of the square beam on the image plane is high when the beam homogenizer is in the imaging condition. When the square beam on the image plane is sharp, the heat affected zone, where the metal target is just heated without any LSP effect because of the laser intensity being below the plasma threshold, can be minimized [6, 13]. In the imaging condition, the square-shaped beam homogenizer not only allows the effective use of energy [13-15] but also ensures that the beam covers the metal target efficiently [1-5].

III. PRELIMINARY SIMULATION

3.1. Simulation Method

In this study, the square-shaped beam homogenizer was configured numerically and the diffraction effect was considered [16], unlike in the previous study in which simulation was performed using the Monte Carlo ray tracing method [7]. The electric field E_2 by the Fresnel diffraction expression with the Fourier convolution theorem can be presented as [17]

$$E_2(x,y) = \mathcal{F}^{-1}\{\mathcal{F}\{E_1(x,y)\,t(x,y)\}\mathcal{F}\{h(x,y)\}\}, \tag{4}$$

where E_1 is the input electric field, $t(x, y)$ is the transmittance function and $h(x, y)$ is the impulse response function. The transmittance function is given by

$$t(x, y) = P(x, y)\, exp\left[-j\frac{k}{2f}(x^2+y^2)\right], \tag{5}$$

where $P(x, y)$ is the square pupil function, k is the wave number and f is the focal length of lenses. The input electric field E_1 is propagated by the impulse response function which given as

$$h(x, y) = \frac{exp(jkz)}{j\lambda z}\, exp\left[\frac{jk}{2z}(x^2+y^2)\right]. \tag{6}$$

The beam propagation calculation through the array lenses should be divided per each lenslet for efficient use of memory for the numerical simulation [16]. The divided electric fields by each lenslet propagate until they meet the condenser lens. From the condenser lens, the divided electric fields are joined and the resultant propagates to the image plane. Because of the significant difference of the field size of condenser lens and image plane, the "Fresnel Two-step propagator" was used in the propagation calculation from the condenser lens to the image plane [17].

The beam data was obtained from -2 to +3 cm at intervals of 0.1 cm near the image plane, and beam distribution over the plasma threshold of the metal target was analyzed at each defocused point. Figure 2(a) shows the simulation method, in which an over the plasma threshold region exists in the integrated beam distribution.

The nonuniform input beam was calculated as approximately 1 cm at full width half maximum by using the moving knife-edge method that integrates pixel intensities through the x and y axes [18]. The beam had a 10 ns pulse width, 532 nm wavelength, and 6.9 J energy per one pulse. Table 1 shows the parameters of the beam homogenizer for the preliminary simulation. The maximum square beam size can be 0.26 cm to perform the LSP with 6.9 J/pulse on the metal target, which has 10 GW/cm^2 plasma threshold [2].

The dashed line in Fig. 2(b) represents the energy efficiency graph (η_E) defined in the previous study [7, 19], with parameters defined in Table 1. As shown in Fig. 2(b), even though the LSP-DOF is calculated as 1.7 cm around the target plane, the LSP-DOF includes the square beam with poor quality (e.g., the 1.3 cm defocused beam at the third inset); this is inappropriate for the LSP. Therefore, we applied the LSP-DOU as the expectable range of a good peening quality, with values below a certain RMS value of the intensity over the plasma threshold of the metal target. The LSP-DOU can exclude the defocused range including improper beam distribution over the plasma threshold despite beam distribution comprising enough energy efficiency. The normalized RMS of the intensity profile defined by ISO 13694(2015) [20] is shown as

$$U_{th}(z) = \frac{1}{H_{av}(z)} \sqrt{\frac{1}{A^i_{th}(z)} \iint [H(x, y, z) - H_{av}(z)]^2\, dxdy}, \tag{7}$$

where $H_{av}(z)$ and $A^i_{th}(z)$ are the averaged intensity distribution and area over the th at location z, respectively. While th is a fraction of the maximum energy density in ISO standard, the th can be regarded as the plasma threshold of the metal target for the LSP. Equation (7) generates the RMS value, which represents the uniformity of intensity over the plasma threshold of the metal target. To define the LSP-DOU, we limited the range of RMS to less than 5% [10]. The solid line in Fig. 2(b) shows the RMS curve around the target from -2 to 3 cm.

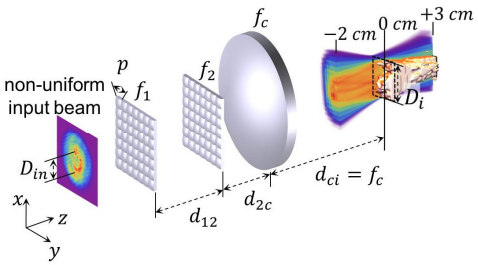

(a)

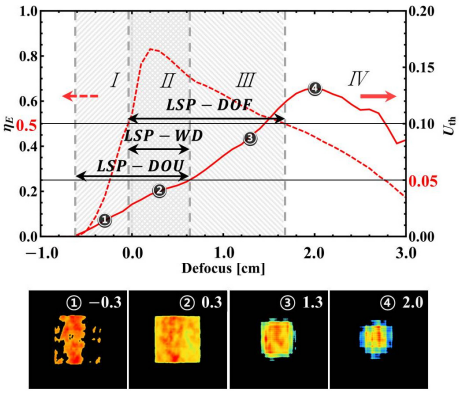

(b)

FIG. 2. (a) The simulation configuration of the beam homogenizer for the metal target with 10 GW/cm^2 plasma threshold and a possible LSP region in the integrated beam distribution (b) The energy efficiency curve (dashed line, η_E) and RMS curve (solid line, U_{th}) along the defocused range from -2 cm to +3 cm, and the beam distributions over the plasma threshold at each defocused position -0.3, 0.3, 1.3, and 2.0 cm from the target.

TABLE 1. Parameters of the preliminary simulation (Unit: [cm])

p	f_1	$f_2 = d_{12}$	d_{2c}	f_c	D_i
0.26	13.0	17.0	25.0	17.0	0.26

3.2. Analysis of the Preliminary Simulation

Note that we analyzed the beam energy efficiency and uniformity only over the plasma threshold beam distribution. Accordingly, the LSP-DOU is defined as the range in zones *I* and *II*. The LSP-DOF is defined as the range in zones *II* and *III*. The overlapped zone *II* is the LSP-WD. The representative insets in Fig. 2(b) show the beam distributions for the LSP for each zone. Zone *I* shows beam distributions over the plasma threshold with both low RMS and energy efficiency. The first inset shows a defective shape but is uniform in plasma-occurring region. Zone *II* shows LSP-WD, which satisfies $\eta_E \geq 0.5$ and RMS < 5%. In this range, the uniform square beam is maintained for LSP with high energy efficiency and low RMS. The second inset shows that the beam has a square-like shape and its uniformity is satisfactory for LSP. The beam distributions in zone *III* have a high energy efficiencies and a high RMS value (the third inset). Furthermore, the beam distributions in zone *IV* have low energy efficiencies and high RMS (the fourth inset). We can expect a good LSP quality in zone *II* and we can regard LSP-WD as an energy efficient and LSP-quality guaranteed range. The LSP-DOU and LSP-WD were calculated as 1.23 and 0.67 cm, respectively, with these pre-simulation parameters. The next section shows our analysis of the effect of some parameters on the LSP-DOU and LSP-WD.

IV. SIMULATION RESULTS AND DISCUSSION

4.1. Parameter Selection

In our previous study, we studied beam-homogenizer parameters related to the LSP-DOF [7]. The parameters can be loosely divided into internal and external parameters. The internal parameters are directly connected to the beam homogenizers, and include the focal lengths of each lens, distances between lenses, and pitch size of the array lens. The external parameters can include the properties of the metal target and conditions of the input beam. In this study, we selected the focal length of the condenser lens (f_c) and the pitch size of the array lens (p) as the internal parameters. These parameters are important because f_c is associated with the DOF and LSP-DOF, and p is involved in beam uniformity [7, 10]. In addition, we selected the plasma threshold as an external parameter. In the previous study, it had been significant in terms of strong relation with LSP-DOF [7].

4.2. The Effect of Increasing f_c

In the first simulation, we changed f_c based on the preliminary simulation parameters (Table 1). The square image size was set to 0.26 cm for the metal target, which has a 10 GW/cm^2 plasma threshold with a 6.9 J/pulse input beam. In the preliminary simulation, f_c = 17.0 cm, which was linearly changed as much as ±6.0 cm in the first simulation. When f_c = 11.0, 17.0, and 23.0 cm, f_2 and d_{12} were changed equally with constant p to fix the square image size according to the imaging condition (Eq. (3)). Table 2 shows the parameters of the first simulation when f_c is changed, while those of second case are a reference. When f_c = 11.0, 17.0, and 23.0 cm, the efficiency curves are shown in Fig. 3(a) and the RMS curves are shown in Fig. 3(b). The trends of the LSP-DOF, LSP-DOU, and LSP-WD are shown in Fig. 3(c). Increase in f_c dramatically increases the LSP-DOF. Moreover, the LSP-DOU is increased as the RMS curve is inclined entirely. The LSP-WD is increased depending on the growth of LSP-DOF and LSP-DOU. The longer the f_c

TABLE 2. Beam homogenizer parameters for changing f_c (unit: [cm])

p	f_1	$f_2 = d_{12}$	d_{2c}	f_c	$LSP-DOF$	$LSP-DOU$	$LSP-WD$
0.26	13.0	11.0	25.0	11.0	1.20	0.65	0.35
		17.0		17.0	1.71	1.23	0.67
		23.0		23.0	2.61	1.54	0.97

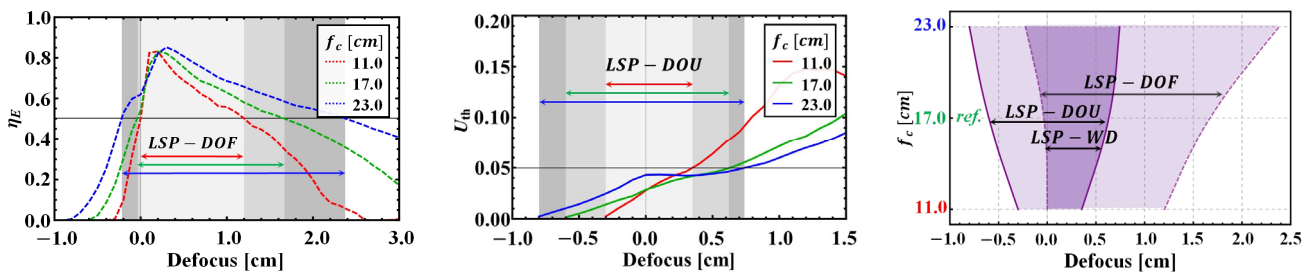

(a) (b) (c)

FIG. 3. Plots of (a) LSP-DOF and (b) LSP-DOU for simulating the changing f_c. (c) Plot of the trends of LSP-DOF, LSP-DOU, and LSP-WD according to changing f_c.

helps the LSP-DOF, the more the LSP-DOU and LSP-WD are lengthened.

4.3. The Effect of Increasing p

In the second simulation, p is changed based on the reference parameters (Table 1). In the preliminary simulation, $p = 0.26$ cm, which was linearly changed as much as ± 0.4 cm in this simulation. The dependent parameters f_2 and d_{12} were changed equally but f_c was set to 17.0 cm to fix the square image size for the metal target with 10 GW/cm^2 plasma threshold. Table 3 shows the parameters, as p is changed to 0.22, 0.26, and 0.30 cm. In Table 3, the second case ($p = 0.26$ cm) is the reference. When $p = 0.22$, 0.26, and 0.30 cm, the efficiency curves are shown in Fig. 4(a) and the RMS curves are shown in Fig. 4(b). Fig. 4(c) shows the trends of LSP-DOF, LSP-DOU, and LSP-WD. With the increases in p, the LSP-DOF is increased slightly. The LSP-WD is generated by the left- and right-side limits of the LSP-DOF and LSP-DOU, respectively. The left-side limit of the LSP-DOU moves to the right side and the slope of the LSP-DOU curve is steeper. In contrast, the LSP-WD decreases when p is increased because p is the chopping size, at which the array lens splits the arbitrary input beam and is strongly connected to the uniformity. An increase of p decreases the LSP-WD.

4.4. The Effect of Decreasing I_{th}

In the last simulation, the plasma threshold (I_{th}) is varied. In this simulation, the square beam designed for the 10 GW/cm^2 plasma threshold hits other metal targets with different plasma thresholds. The parameters of the square-shaped beam homogenizer are the same as those in the reference, that is, the parameters of the preliminary simulation. The plasma threshold was 10 GW/cm^2 in the preliminary simulation; however, in this simulation, the plasma threshold was diminished as much as 1.2-2.4 GW/cm^2, that is, it was changed to 10.0, 8.8, and 7.6 GW/cm^2. Table 4 shows the parameters of this simulation, and the first case is the reference.

When the I_{th} is changed to 10.0, 8.8, and 7.6 GW/cm^2, Figs. 5(a) and (b) show the efficiency and uniformity changes, respectively. Moreover, Fig. 5(c) shows the trends of LSP-DOF, LSP-DOU and LSP-WD. The energy efficiency is improved and the LSP-DOF increases when the I_{th} value is reduced, similar to the results in our previous study [7]. However, the LSP-DOU level increases entirely. When $I_{th} =$ 8.8 GW/cm^2, the LSP-DOU is longer than when $I_{th} = 10$ GW/cm^2 but shorter than when $I_{th} = 7.6$ GW/cm^2. Although LSP-DOF dramatically increases with low I_{th}, the LSP-WD

TABLE 3. Beam homogenizer parameters for changing p (unit: [cm])

p	f_1	$f_2 = d_{12}$	d_{2c}	f_c	$LSP-DOF$	$LSP-DOU$	$LSP-WD$
0.22	13.0	14.4	25.0	17.0	1.40	1.88	0.97
0.26		17.0			1.71	1.23	0.67
0.30		19.6			1.84	1.20	0.46

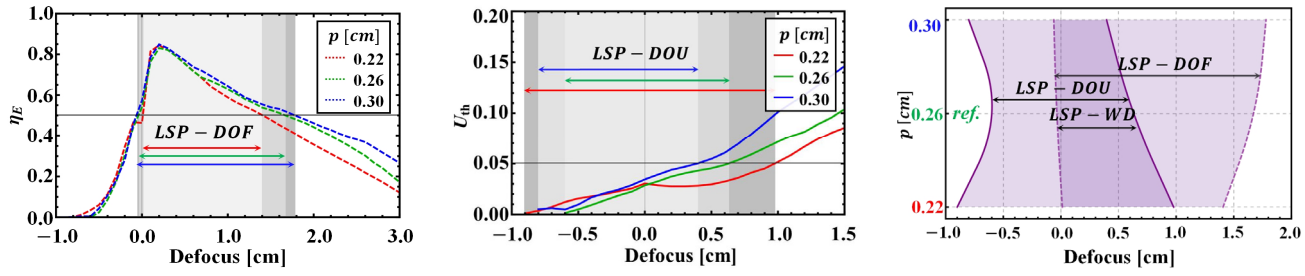

(a) (b) (c)

FIG. 4. Plots of (a) LSP-DOF and (b) LSP-DOU for simulation of changing p. (c) Plot of the trends of LSP-DOF, LSP-DOU, and LSP-WD according to varying p.

TABLE 4. Beam homogenizer parameters for changing I_{th} (unit: [cm])

I_{th} [GW/cm^2]	p	f_1	$f_2 = d_{12}$	d_{2c}	f_c	$LSP-DOF$	$LSP-DOU$	$LSP-WD$
10.0	0.26	13.0	17.0	25.0	17.0	1.71	1.23	0.67
8.8						2.63	1.66	0.82
7.6						3.70	1.03	0.16

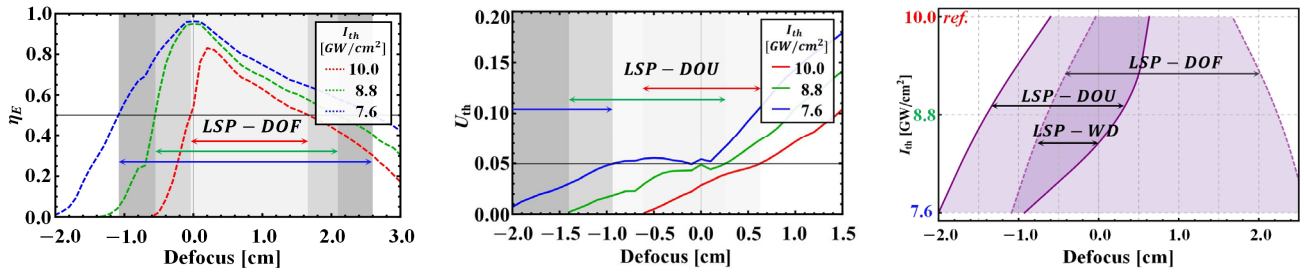

(a) (b) (c)

FIG. 5. Plots of (a) LSP-DOF and (b) LSP-DOU for simulating the changing of I_{th}. (c) Plot of the trends of LSP-DOF, LSP-DOU, and LSP-WD according to varying I_{th}.

drastically decreases because of the increasing RMS level and decreasing LSP-DOU. It is necessary to adjust the square beam size or input energy to set the proper intensity when the type of the metal target is changed. Immediate control of the square beam size is advantageous not only for the peening quality and LSP-WD but also for the LSP working efficiency [7].

V. CONCLUSION

The LSP-DOF by itself is incomplete in defining the WD of the square-shaped beam homogenizer for LSP. The LSP-DOU was obtained by applying the beam uniformity over the plasma threshold. The LSP-WD is the range where the LSP-DOF and LSP-DOU overlap. The LSP-DOF, LSP-DOU, and LSP-WD show different trends depending on the parameters. The longer focal length of the condenser lens increases both the LSP-DOF and LSP-DOU, thus increasing LSP-WD. The pitch of the array lens does not have a significant effect on the LSP-DOF; however, with respect to the uniformity, the larger pitch size reduces the uniformity and LSP-DOU, thereby reducing the LSP-WD. LSP-DOF is increased as the plasma threshold of the metal target is decreased; however, the LSP-DOU and LSP-WD decrease because uniformity is reduced. The square-shaped beam homogenizer for the LSP should be designed to have high efficiency, high uniformity, and long LSP-WD. This designed square-shaped beam homogenizer will contribute to the improvement of the LSP working efficiency, quality, and productivity. In the future, we will compare experimental results and the abovementioned simulation results.

ACKNOWLEDGMENT

We thank Professor Jongmin Lee for his care and guidance. This work was supported by the Industrial Strategic Technology development program, 10048964. The development of the 125 J·Hz laser system for laser peening was funded by the Ministry of Trade, Industry & Energy (MI, Korea).

REFERENCES

1. M. Schwartz, *New materials processes, and methods technology* (CRC Press, Boca Raton, FL, USA, 2006).
2. A. K. Gujba and M. Medraj, "Laser peening process and its impact on materials properties in comparison with shot peening and ultrasonic impact peening," Materials **7**, 7925-7974 (2014).
3. J. E. Rankin, M. R. Hill, and L. A. Hackel, "The effects of process variations on residual stress in laser peened 7049 T73 aluminum alloy," Mater. Sci. Eng. A **349**, 279-291 (2003).
4. P. Crooker and T. Lian, "Materials reliability program: Technical basis for primary water stress corrosion cracking mitigation by surface stress improvement (MRP-267, Revision 1)," EPRI, Palo Alto, CA, USA, (2012).
5. Z. W. Cao, S. L. Gong, and Y. Gao, "Characterization of TC17 titanium alloy treated by square-spot laser shock peening," Adv. Mat. Res. **652-654**, 2378-2383 (2013).
6. R. S. Patel and A. Tamhankar, "Beam profile effect for thin film solar cell scribing," Industrial laser solutions for manufacturing, November, 1 (2010).
7. T. Kim, S. Hwang, K. H. Hong, and T. J. Yu, "Analysis of the square beam energy efficiency of a homogenizer near the target for laser shock peening," J. Opt. Soc. Korea **20**, 407-412 (2016).
8. J. Lin, L. Xu, S. Wang, and H. Han, "Theoretical analysis of lens array for uniform irradiation on target in multimode fiber lasers," Chin. Opt. Lett. **12**, 101402 (2014).
9. X. Jiang, J. Li, H. Li, Y. Li, and Z. Lin, "Uniform irradiation of adjustable target spots in high-power laser driver," Appl. Opt. **50**, 5213-5220 (2011).
10. M. Zimmermann, N. Lindlein, R. Voelkel, and K. Weible, "Microlens laser beam homogenizer - from theory to application," Proc. SPIE **6663**, 1-13 (2010).
11. F. M. Dickey and S. C. Holswade, *Laser Beam Shaping Theory and Techniques* (CRC Press, Boca Raton, FL, USA, 2014).
12. Y. Jin, A. Hassan, and Y. Jiang, "Freeform microlens array homogenizer for excimer laser beam shaping," Opt. Express **24**, 24846-24858 (2016).
13. G. Račiukaitis, E. Stankevičius, P. Gečys, M. Gedvilas, C. Bischoff, E. Jaeger, U. Umhofer, and F. Volklein, "Laser processing by using diffractive optical laser beam shaping," J. Laser Micro Nanoen **6**, 37-43 (2011).
14. R. D. Schaeffer, *Fundamentals of Laser Micromachining*,

(CRC Press, Boca Raton, FL, USA, 2012).
15. J. Bovatsek and R. S. Patel, "High-power, nanosecond-pulse Q-switch laser technology with flattop beam-shaping technique for efficient industrial laser processing," (http://www.spectra-physics.com/assets/client_files/files/documents/29436.pdf).
16. S. Hwang, T. Kim, J. Lee, and T. J. Yu, "Design of square-shaped beam homogenizer for petawatt-class Ti:sapphire amplifier," Opt. Express **25**, 9511-9520 (2017).
17. D. Voelz, *Computational Fourier Optics: A MATLAB Tutorial* (SPIE Press, Bellingham, WA, USA, 2011).
18. I. Eriksson, "The monitoring of a laser beam." Master's Thesis, Mid Sweden University (2005).
19. Z. Kuang, J. Li, S. Edwardson, W. Perrie, D. Liu, and G. Dearden, "Ultrafast laser beam shaping for material processing at imaging plane by geometric masks using a spatial light modulator," Opt. Lasers Eng **70**, 1-5 (2015).
20. ISO 13694:2015, Optics and Optical Instruments-Lasers and Laser Related Equipment-Test Method for Laser Beam Power (Energy) Density Distribution, (2015).